



Interaction of Zn with Losartan. Activation of Intrinsic Apoptotic Signaling Pathway in Lung Cancer Cells and Effects on Alkaline and Acid Phosphatases

Valeria R. Martínez¹ · María V. Aguirre² · Juan S. Todaro² · Oscar E. Piro³ · Gustavo A. Echeverría³ · Luciana G. Naso¹ · Evelina G. Ferrer¹ · Patricia A. M. Williams¹

Received: 14 February 2018 / Accepted: 3 April 2018 / Published online: 12 April 2018

© Springer Science+Business Media, LLC, part of Springer Nature 2018

Abstract

A new losartan [2-butyl-5-chloro-3-[[4-[2-(2H-tetrazol-5-yl)phenyl]phenyl]methyl]imidazol-4-yl]methanol zinc(II) complex [Zn(Los)Cl], was synthesized and characterized. The crystal structure was determined by x-ray diffraction methods. When aqueous solutions of the ligand and the metal were mixed, the known and more soluble powder [Zn(Los)₂].3H₂O (ZnLos) complex has been obtained. The interactions with phosphatases showed a concerted mechanism displayed by the Zn ions and ZnLos up to 500 μM concentration: a decrease of the acid phosphatase (AcP) associated with an increase in the alkaline phosphatase (ALP) activities. The complex and ZnSO₄ showed a cytotoxic behavior on human lung A549 cancer cell line at concentrations higher than 75 μM with reactive oxygen species (ROS) generation and GSH (and GSH/GSSG ratio) depletion. Apoptotic cells were observed using terminal deoxynucleotidyl transferase dUTP nick-end labeling (TUNEL) method, a mechanism accompanied by upregulation of BAX protein, downregulation of Bcl-XL and release of caspase-3. The BAX/Bcl-XL ratio was found to be significantly higher in cells exposure to ZnLos than cells treated with ZnSO₄, in agreement with the higher apoptotic percentage of cells found for the complex. Cell death was found to be produced by apoptosis and no necrosis has been observed. On the contrary, losartan exerted low effects on phosphatases, produced some reduction of cancer cell viability (concentrations > 250 μM, number of apoptotic cells similar to the basal) with low ROS depletion, without alteration of the GSH/GSSG and low BAX/Bcl-XL ratios. In the MRC-5, normal lung fibroblasts cell line only ZnSO₄ at concentrations higher than 200 μM displays cytotoxic effects.

Keywords Losartan · Zinc coordination · Enzymatic inhibition · Anticancer mechanism

Introduction

Lung cancer is one of the leading causes of death around the world and non-small cell lung cancer (NSCLC) accounts for

about 85% of this type of cancer [1]. On the other hand, the renin-angiotensin system regulates blood pressure and the angiotensin receptor blockers (ARBs or sartans) have been designed to selectively binding and blocking to the angiotensin II type 1 (AT1) receptor [2], reducing the vasoconstrictor action of the angiotensin II peptide. Recent studies showed that the AT1 receptors are expressed in the A549 human lung adenocarcinoma cells and that the treatment with an AT1 receptor antagonist could inhibit the proliferation of lung cancer cell lines [3]. Therefore, medications may provide synergistic effects to existing chemotherapies by reducing Ang II-mediated mitogenesis and angiogenesis [4]. To introduce structural modifications to the sartans (whose functional groups bear multiple binding sites and strong coordinating ability), we have synthesized coordination complexes with the biometal copper(II) that allow the improvement of some of the biological properties or the ARBs such as the anticancer effects [5].

Electronic supplementary material The online version of this article (<https://doi.org/10.1007/s12011-018-1334-x>) contains supplementary material, which is available to authorized users.

✉ Patricia A. M. Williams
williams@quimica.unlp.edu.ar

¹ Centro de Química Inorgánica (CEQUINOR-CONICET-CICPBA-UNLP), 120 N° 1465, La Plata, Argentina

² Laboratorio de Investigaciones Bioquímicas, Facultad de Medicina, UNNE, Moreno, 1240 Corrientes, Argentina

³ Departamento de Física, Facultad de Ciencias Exactas, Universidad Nacional de La Plata y IFLP (CONICET, CCT La Plata), C.C. 67, 1900 La Plata, Argentina

Zinc is a trace essential element in which deficiency includes growth retardation and cell-mediated immune dysfunctions. Zinc deficiencies in diets can also contribute in the damage of DNA that increase risk for cancer development [6]. Zinc treatment enhances cell-mediated immunity and displays protective mechanisms against DNA damage which may be a possible mechanism for its anticancer activity [7]. Moreover, zinc supplementation decreases angiogenesis and the induction of inflammatory cytokines hence increasing apoptosis in cancer cells [8]. The anticancer effects of Zn(II) ions have been determined in several cancer cell lines including, for instance, non-small-cell lung cancer cells [9].

Considering that sartans have the potential to reduce zinc levels in hypertensive patients, yielding an increase in urinary Zn excretion and a decrease of serum Zn levels [10], we started the study of the synthesis of a new Zn-sartan complexes and the determination of some of the biological effects. Therefore, we have introduced newer therapeutic strategies to supply the biometal Zn together with the sartan drug, and avoid the alteration of the metal concentrations in specific body organs and/or entire body by the generation of a metal complex with sartan. The strategy of the combination of Zn(II) and sartan in a coordination compound has been developed to bring additional biological properties during the administration of the antihypertensive drugs. In fact, the Zn/azilsartan complex previously prepared in our group [11] produced an improvement of the anticancer effect of the parent drug, azilsartan.

One of the orally effective pharmaceutical drugs used for the treatment of arterial hypertension (ARB) is losartan potassium, the potassium salt of [2-butyl-5-chloro-3-[[4-[2-(2H-tetrazol-5-yl)phenyl]phenyl]methyl]imidazol-4-yl]methanol (from now on, losartan, Los) (Fig. 1). The structure of losartan consisted in a biphenyltetrazole ring system attached to a substituted imidazole ring through a methylene spacer (Fig. 1). The thermal, spectroscopic characterization, antioxidant evaluation (against 1,1-diphenyl-picrylhydrazyl, DPPH) and the pyrolysis [12] and the complex formation equilibria of losartan with Zn(II) [13], $[\text{Zn}(\text{Los})_2] \cdot 3\text{H}_2\text{O}$ (ZnLos), have recently been reported. Here, we report some spectroscopic characterizations and the biological studies of this solid complex. In an attempt to obtain single crystals suitable for structural determinations using gel diffusion techniques, a new Zn(II) complex with losartan and chloride ions

in its coordination sphere, $[\text{Zn}(\text{Los})\text{Cl}]$ has been obtained. Due to the insolubility of the $[\text{Zn}(\text{Los})\text{Cl}]$ complex, the biological determinations were performed using the known $[\text{Zn}(\text{Los})_2] \cdot 3\text{H}_2\text{O}$ complex.

Phosphoregulation is involved in many biological events and often occurs as a network-like cascade, in which the activity of one phosphatase or kinase is dependent on the upstream activity of another. A considerable rise in alkaline phosphatase (ALP) activity is produced in various types of malignant tumors and is used as a tumor marker [14]. While ALP contains Zn ions, the addition of concentrations lower than 1 mM Zn(II) could increase its enzymatic activity. However, acid phosphatases (AcP) are being inhibited by Zn(II) [15]. Herein, we report our findings on the Zn(II) complex, the metal and the ligand on their action exerted on AcP and ALP. Additionally, we determined their possible anticancer activities in a human lung A549 cell line and the mechanism of action: cellular reactive oxygen species (ROS) generation and glutathione (GSH) depletion with the concomitant oxidation of GSH to GSSG and presence of apoptotic or necrotic cells (terminal deoxynucleotidyl transferase dUTP nick-end labeling (TUNEL), ratio of the apoptotic regulators proteins BAX to Bcl-XL, caspase-3 activation). Data are presented and discussed above. The cytotoxic effect of the compounds against human normal lung fibroblast (MRC-5) cell line has also been determined.

Experimental

Materials and Methods

All chemicals were of analytical grade and used without further purification. Losartan, potassium salt was purchased from Parafarm and Zinc(II) nitrate (Merck) was used as supplied. A sodium silicate solution (14% NaOH-27% SiO₂, SiO₂·NaOH, Sigma-Aldrich) was used for the diffusion method. Infrared spectra of powdered samples were measured with a Bruker IFS 66 FTIR-spectrophotometer from 4000 to 400 cm⁻¹ using the KBr pellet technique. FT-Raman spectra were measured using the FRA 106 Raman accessory with germanium detector operating at liquid nitrogen temperature. A continuous-wave Nd/YAG laser working at 1064 nm was employed for Raman excitation. Elemental analyses for carbon, hydrogen and nitrogen were performed using a Carlo Erba EA 1108 analyzer. Thermogravimetric analysis (TGA) were measured with a Shimadzu system (model TG-50), working in an oxygen flow of 50 mL/min and at a heating rate of 10 °C/min. Sample quantities ranged between 5 and 10 mg. Electronic absorption spectra were recorded on a Hewlett-Packard 8453 diode-array spectrophotometer, using 1-cm quartz cells. Fluorescence spectra were measured using a Shimadzu RF-6000 spectrophotometer. The molar conductance of the complex was measured on a Conductivity TDS Probe - 850,084,

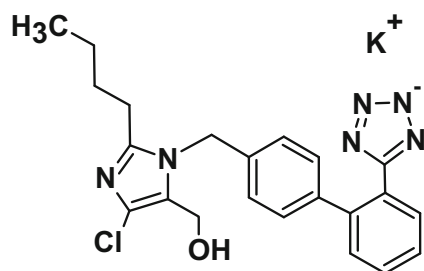


Fig. 1 Losartan structure

Sper Scientific Direct, using 10^{-3} M DMSO or aqueous solutions.

Synthesis of $[\text{Zn}(\text{Los})_2]\cdot 3\text{H}_2\text{O}$

Aqueous solutions of losartan (1 mmol, 10 mL) and $\text{Zn}(\text{NO}_3)_2$ (0.5 mmol, 5 mL) were mixed at room temperature at a final pH value of 7. The white precipitate was filtered, washed with distilled water, and dried in an oven at 60 °C. Attempts to grow single crystals using different experimental techniques failed. Elemental analysis (%): Calc for $\text{C}_{44}\text{H}_{50}\text{Cl}_2\text{N}_{12}\text{O}_5\text{Zn}$ (963.3): C, 54.8; H, 5.2; and N, 17.5. Found: C, 54.7; H, 5.2; and N, 17.5. The three labile water molecules are lost at 107 °C ($\Delta\omega\%$ calcd, 5.6; $\Delta\omega\%$, exp. = 5.5). UV-Vis spectrum (EtOH) λ_m 225 and 250 nm; $\epsilon = 2.5 \times 10^4 \text{ M}^{-1}/\text{cm}^{-1}$ and $1.2 \times 10^4 \text{ M}^{-1}/\text{cm}^{-1}$, respectively. Fluorescence spectrum (1×10^{-5} M, EtOH) $\lambda_{ex} = 295$ nm; $\lambda_{em} = 370$ nm. Diffuse reflectance spectrum = 259 nm, 283 sh.

Synthesis of $[\text{Zn}(\text{Los})\text{Cl}]$

To obtain the crystal structure of the ZnLos, complex single crystals suitable for x-ray determinations were grown in U-tubes by the gel diffusion method. The bottom of the U-tube was filled with silicate gel (sodium silicate 5% aqueous solution with the addition of 50% HCl up to pH 7). One side-arm of the tube was filled with an aqueous solution of losartan (1 mmol, 10 mL) and the other with a Zn nitrate aqueous solution (0.5 mmol, 5 mL). Over a period of 6 months, single crystals grew inside the gel. Instead of the desired $[\text{Zn}(\text{Los})_2]\cdot 3\text{H}_2\text{O}$ complex, a new compound of Zn(II) with losartanate bonded to one chloride anion in its coordination sphere (due to the presence of chloride ions in the silicate gel) has been obtained. Diffuse reflectance spectrum = 254 nm, 280 sh.

Single-Crystal X-ray Diffraction Data

The structural determinations of the $[\text{Zn}(\text{Los})\text{Cl}]$ complex were performed on an Oxford Xcalibur Gemini, Eos CCD diffractometer with graphite-monochromated $\text{CuK}\alpha$ ($\lambda = 0.154184 \text{ \AA}$) radiation. X-ray diffraction intensities were collected (ω scans with ϑ and κ -offsets), integrated and scaled with CrysAlisPro [16] suite of programs. The unit cell parameters were obtained by least-squares refinement (based on the angular settings for all collected reflections with intensities larger than seven times the standard deviation of measurement errors) using CrysAlisPro. Data were corrected empirically for absorption employing the multi-scan method implemented in CrysAlisPro. The structure was solved by the intrinsic phasing method implemented in SHELXT of the SHELX suit of programs [17] and refined by full-matrix least-squares with SHELXL of the same package. The hydrogen atoms were

located in a difference Fourier map and all but the ones of $-\text{CH}_3$ group were refined at their found positions with isotropic displacement parameters. The methyl H atoms were refined with the riding model as a rigid group allowed to rotate around the C– CH_3 bond such as to maximize the sum of the residual density at the calculated positions. The methyl group converged to a staggered rotational conformation. Crystal data, data collection procedure, structure determination methods, and refinement results are summarized in Table 1.

Behavior on Phosphatases Activities

Alkaline Phosphatase

The effect of the Zn(II) cation, losartan, and the ZnLos complex on ALP activity was determined spectrophotometrically. The reaction was started by the addition of the substrate (p-NPP) and the generation of p-nitrophenol was monitored by the absorbance changes at 405 nm [18]. Briefly, the experimental conditions for ALP-specific activity measurement were as follows: 1 $\mu\text{g}/\text{mL}$ of bovine intestinal ALP and 5 mM of p-NPP were dissolved in the incubation buffer (55 mM glycine + 0.55 mM MgCl_2 , pH = 10.5) and held for 4 min. The effects of the compounds were determined by addition of different concentrations (1–500 μM) of each one to the pre-incubated mixture. The compounds were dissolved in DMSO and the stock solutions were diluted in the buffer giving a final concentration of DMSO less than 1%. The effect of each concentration was tested in three independent experiments at least by triplicated. The initial rate, in absence of any compound (V_0), was determined as the rate of p-NPP hydrolysis at 37 °C and pH = 10.5. V_i values were determined like V_0 but in the presence of the different concentrations of each of the investigated systems. Data were expressed as mean \pm SEM. An analysis of variance (one-way ANOVA) was applied to compare the means of multiple groups of measured data. Significance was defined as $p < 0.05$.

Acid Phosphatase

Acid phosphatase (AcP) inhibition test was performed according to Blum and Schwedt procedures [19] using acid phosphatase (AcP from potato, product number P-3752, Sigma Chemical Co. (St. Louis, MO)). The stock solution of the enzyme was prepared by mixing 12.5 mg of the 0.25 U/mL acid phosphatase powder in 2.0-mL acetate buffer (pH 5.60). The stock solution of the compounds (100 μL in DMSO) was diluted in 1.9 mL of the buffer and 0.170 g of the substrate p-NPP were dissolved in distilled water (2.5 mL). A volume of 0.50 mL of each compound solution was mixed with 0.10 mL of the enzyme solution and 1.00 mL of buffer. The mixture was kept at 25 °C for 20 min (incubation time). Then, the substrate (0.10 mL) has been added. The reaction was stopped

Table 1 Crystal data and structure refinement results for chlorolosartanatenzinc(II) complex

Empirical formula	C ₂₂ H ₂₂ Cl ₂ N ₆ O Zn	
Formula weight	522.72	
Temperature	293(2) K	
Wavelength	1.54184 Å	
Crystal system	Monoclinic	
Space group	P 2 ₁ /n	
Unit cell dimensions	<i>a</i> = 12.5723(7) Å	<i>c</i> = 20.0046(10) Å
	<i>b</i> = 9.4476(6) Å	
	<i>β</i> = 92.543(5)°	
Volume	2373.8(2) Å ³	
Z, density (calculated)	4, 1.463 Mg/m ³	
Absorption coefficient	3.725 mm ⁻¹	
<i>F</i> (000)	1072	
Crystal size	0.053 × 0.094 × 0.118 mm ³	
ϑ-range for data collection	4.073 to 72.473°	
Index ranges	−12 ≤ <i>h</i> ≤ 15, −11 ≤ <i>k</i> ≤ 7, −23 ≤ <i>l</i> ≤ 24	
Reflections collected	10,795	
Independent reflections	4640 [<i>R</i> (int) = 0.0559]	
Observed reflections	3009	
Completeness to ϑ = 67.684°	100.0%	
Refinement method	Full-matrix least-squares on <i>F</i> ²	
Data/restraints/parameters	4640:0:366	
Goodness-of-fit on <i>F</i> ²	1.004	
Final <i>R</i> indices ^a [<i>I</i> > 2σ(<i>I</i>)]	<i>R</i> 1 = 0.0501, <i>wR</i> 2 = 0.1121	
<i>R</i> indices (all data)	<i>R</i> 1 = 0.0903, <i>wR</i> 2 = 0.1349	
Largest diff. peak and hole	0.369 and −0.270 e/Å ⁻³	

$$^a R_1 = \frac{\sum \|F_o\| - \|F_c\|}{\sum \|F_o\|}, wR_2 = \frac{[\sum w(|F_o|^2 - |F_c|^2)^2 / \sum w(|F_o|^2)^2]^{1/2}}$$

with the addition of 0.50 mL of a 0.5 M sodium hydroxide solution. The final concentration of DMSO resulted less than 1%. The enzymatic activity was calculated by the measurement of the absorbance of 4-nitrophenolate at 405 nm against a blank prepared without the enzyme. Three independent replicates of each point were measured. In both experiments, 100% of the enzyme activity is assigned to a basal measurement containing all the reaction media including the same volume of DMSO in all the tests. It is worthy to mention that the presence of that very low quantity of DMSO did not affect the enzyme activity. Data were expressed as mean ± SEM. An analysis of variance (one-way ANOVA) was applied to compare the means of multiple groups of measured data. Significance was defined as $p < 0.05$.

Cellular Determinations

Cell Culture

Human alveolar carcinoma cell line (A549) was used in cytotoxicity studies. Cells were cultured in Dulbecco's modified Eagle's Medium (DMEM) supplemented with 5% (v/v) fetal

bovine serum (FBS) and 100 U/mL penicillin-streptomycin, at 37 °C in a humidified incubator with 5% CO₂. At 85% confluence, cells were harvested using PBS-EDTA and suspended at a final concentration of 2 × 10⁶ cells/mL into 6- and 48-well plates and 35-mm dishes, respectively, according to the selected experiment. To examine the effect of the compounds, cells were treated with ZnSO₄, losartan, and ZnLos at different concentrations and then they were assessed in several assays.

Cell Viability Assay

Human lung A549 cancer and normal human lung fibroblast (MRC-5) cells were cultured in 48-well plates. After 24 h of incubation, cells were exposed at different concentrations of ZnSO₄, losartan, and ZnLos (0, 2.5, 5, 10, 25, 50, 75, 100, 250, and 500 μM). Then, cell viability was determined through the 3-(4,5-dimethylthiazol-2-yl)-2,5-diphenyltetrazolium bromide (MTT) assay [20]. A volume of 250 μL of MTT solution was added to each well in an amount equal to 10% of culture volume and cells were incubated for 1.5 h at 37 °C until a purple-colored formazan product developed. The

formazan precipitate was dissolved in acidified isopropanol and has been vigorously stirred until dissolution. The absorbance was measured by UV-Vis spectroscopy at 560 nm.

Reactive Oxygen Species Assay

Intracellular reactive oxygen species (ROS) generation by the compounds was evaluated using dihydrorhodamine 123. This probe passively enters the cell and is oxidized to cationic rhodamine 123. The ROS level was measured by a fluorometric quantitative assay [21]. Briefly, 2×10^4 cells/mL were seeded in 48-well plates and were incubated with ZnSO₄, losartan, and ZnLos (0–500 μ M). Cultured cells were washed with PBS before being incubated in 200 μ L of a solution of 10 μ M DHR 123 for 30 min at 37 °C under light protection. Afterwards, cells were lysed with 0.1% Triton X-100. The fluorescence spectra were recorded at 485-nm excitation and 520-nm emission wavelengths. The proteins were measured according to Bradford technique [22]. Results were presented as the percentage of fluorescence intensity relative to the basal measurements \pm SD.

Estimation of Cell GSH and GSSG Content

A modification of Hissin and Hilf's method [23] was used for the determination of reduced (GSH) and oxidized glutathione (GSSG) content in treated A549 cells. The amounts of both compounds were estimated fluorometrically after the reaction with o-phthalaldehyde (OPT). Cells exposed to 0–500 μ M of ZnSO₄, losartan, and ZnLos were treated with 0.1% Triton X-100, and 100 μ L of the lysates were used to determine the GSH, GSSG, and protein content. GSH selectively reacted with OPT (10 mg/mL in methanol) at pH 8.0 (ice-cold 0.1 M Na₂HPO₄–0.005 M EDTA buffer), whereas after the addition of 0.04 mM N-ethyl maleimide (NEM) in the lysates fractions, only GSSG reacted with OPT at pH 12.0 (0.1 N NaOH). Protein contents in each cellular extract were quantified using the Bradford assay. Standard concentrations of GSH and GSSG (0.05–1.0 μ g/mL) were used. The fluorescence spectra were recorded at 350-nm excitation and 420-nm emission wavelengths. The concentrations in micrograms per milligrams were calculated from the respective calibration curves. The ratio GSH/GSSG was expressed as a percentage of the basal for all the experimental conditions.

Apoptosis Assay

The terminal deoxynucleotidyl transferase (dUTP) nick-end labeling (TUNEL assay) were used to detect DNA strand breaks during apoptosis [24]. A549 cells were seeded in slides into 35-mm dishes. After 24 h of treatment with 500 μ M of ZnSO₄, losartan, and ZnLos, slides were fixed in 4% paraformaldehyde and permeabilized with proteinase K 15 μ g/mL in

10 mM Tris-buffer. TUNEL assay was performed using an *in situ* Cell Death Detection Kit (Roche, Indianapolis, IN, USA) according to the manufacturer's instructions. For positive controls, sections were treated with 0.7 mg/mL DNase I (Sigma-Aldrich) for 15 min before treatment with terminal deoxynucleotidyl transferase (TdT). This enzyme was replaced with the same volume of distilled water in negative controls. Labeled cells were observed and photographed under a fluorescence microscope (Olympus CX-35 equipped with a Coolpix Digital camera) at $\times 40$ magnification. Cells were considered TUNEL-positive when nuclei cells exhibit bright green fluorescence. The apoptotic index (AI) was expressed as the percentage of TUNEL-positive cells per 1000 examined A549 cells.

Immunocytochemistry

A549 cells were grown over coverslips into 35-mm dishes for 24 h. Cells were treated with ZnSO₄, losartan, and ZnLos (500 μ M) for 24 h were fixed in 4% paraformaldehyde for 10 min at room temperature. Cells were quenched for 10 min with 3% hydrogen peroxide in methanol. Then, they were permeabilized with 1% Triton X-100 and stirred during 10 min. Slides were rinsed with 0.5% PBS and PBS-Tween. The following primary antibodies were used: Bcl-XL, BAX, and caspase 3 (Santa Cruz Biotechnology, Inc., Santa Cruz, CA). They were diluted 1:50 in PBS and incubated overnight at humidified atmosphere. Immunostaining was performed using a Dako linked streptavidin-biotin + horseradish peroxidase (LSAB+/HRP) kit (Dako Cytomation) followed by the application of a chromogen 3,3'-diaminobenzidine (DAB) (Dako kit) according to manufacturer's instructions. All negative controls were obtained by excluding the primary antibody from the reaction. Samples were then counter-stained with hematoxylin and visualized under a light microscope. Images were taken using an Olympus Coolpix-microdigital camera fitted on a CX-35 microscope (Olympus, Japan) [25].

Western Blot Analysis

BAX and Bcl-XL expression were determined by immunoblotting analysis from whole A549 cell extracts. Briefly, A549 cell cultures were incubated with ZnSO₄, losartan, and ZnLos (500 μ M) for 24 h. Homogenates were obtained by treating monolayers with 200 μ L of RIPA buffer (50 mM Tris, 150 mM NaCl, 2.5 mg/mL deoxycholic acid, 1 mM ethylene glycol-bis(β -aminoethyl ether)-N,N,N',N'-tetraacetic acid (EGTA), 10 μ g/mL Nonidet-40 (pH 7.4), supplemented with protease inhibitors: 2.5 μ g/mL leupeptin, 0.95 μ g/mL aprotinin, and 2.5 mM phenylmethylsulfonyl fluoride (PMSF) [26]. Protein content in lysates was determined by Bradford method. Proteins (25 μ g) were resolved by 12% SDS-PAGE and transferred to a nitrocellulose membrane

(Bio-Rad, CA, USA). Membranes were blocked and then were incubated overnight at 4 °C with the following primary antibodies: anti-BAX (1: 750) and anti-Bcl-XL (1: 1000) (Santa Cruz Biotechnology, Santa Cruz, CA, USA) or anti- β actin (Sigma-Aldrich). The technique was followed with incubation for 1 h at room temperature with horseradish peroxidase-conjugated secondary antibodies (Jackson ImmunoResearch Inc., USA). β actin detection was used to normalize immunoblottings. Immunocomplexes were detected by an Opti4CN (4-chloro-1-naphthol) kit (Bio-Rad, CA, USA). Band optical density (OD) was analyzed using Scion-beta 2 image software and results were expressed as the ratio: (protein of interest OD/ β -actin OD) \times 100. All experiments have been performed by triplicate and a representative immunoreactive band of one experiment is shown.

AO/EtBr Staining

Acridine orange/ethidium bromide (AO/EtBr) staining was carried out to detect morphological evidence of apoptosis and necrosis. While AO is a vital dye that stains both live and dead cells and makes the nuclei appear green, EtBr only stains cells that have lost membrane integrity (nucleus in red). Early apoptotic cells stain green and contain bright dots in the nuclei. Late apoptotic cells also incorporate EtBr and show condensed and often fragmented nuclei. Necrotic cells also stain in orange, but present nuclear morphology resembling that of viable cells [27]. The stock solution of AO was prepared dissolving 5 mg in 1 mL of ethanol and stored in the refrigerator. The same procedure was made for EtBr. To prepare the staining solution 20 μ L of AO and 20 μ L of EtBr were added to 960 μ L of PBS. Briefly, A549 cells were seeded into 100-mm dishes. After 24 h of treatment with ZnSO₄, losartan, and ZnLos (500 μ M), the supernatant (medium and floating A549 cells) were transferred to 15-mL tubes. The rest of the adherent cells were detached with PBS-EDTA. The supernatant and the detached cells from the same sample were pooled together in the 15-mL tubes. A549 cells were pelleted by centrifugation at 1000 RPM for 5 min and washed with 1 mL of cold PBS. Cell pellets were then re-suspended with 1 mL of the staining solution. The cells were then washed with PBS and examined under a fluorescence microscope (Olympus CX-35) at \times 100 magnification.

Statistical Analysis

Data are expressed as the mean \pm standard error (SE). The Sigma plot software package was used for statistical analysis. An analysis of variance (one-way ANOVA) was applied to compare the means of multiple groups of measured data. Significance was defined as $p < 0.05$.

Results and Discussion

Description of the Structure of [Zn(Los)Cl]

Figure 2 shows an ORTEP [28] drawing of the supra-molecular zinc(II) complex and the corresponding bond distances and angles around the metal are given in Table 2. The losartan ligand is negatively charged by loss of the proton at the tetrazole CN₄H ring. The zinc(II) ion is in a tetrahedral ZnN₃Cl environment, coordinated to the imidazole pyridine-like N atom along its electron lone pair [d(Zn–N1) = 2.016(3) Å], to two lateral N's of tetrazole heterocyclic group [d(Zn–N5) = 2.041(3) Å, d(Zn–N6) = 2.034(3) Å], each belonging to two, inversion-related losartan anions, and to a chloride ion [d(Zn–Cl) = 2.211(1) Å]. L–Zn–L bond angles in the complex are in the range from 103.8(1)° to 116.9(1)°. As can be appreciated in Fig. 2, neighboring ZnN₃Cl complexes are bridged by the above-mentioned pair of losartan anions through their tetrazole rings to conform a local center-symmetric dimer in the lattice, (ZnN₃Cl)₂, with a Zn...Zn distance of 3.842(1) Å. The coordination bonding gives rise to a three-dimensional supra-molecular structure that extends throughout the crystal.

The supra-molecular complex is further stabilized in the solid by an intermolecular OH...N3' bond involving as donor the oxhydryl group of a losartan ligand and as acceptor the tetrazole N3 nitrogen of a neighbor ligand [d(O...N3') = 2.917(5), \angle (O–H...N3') = 173(7)°].

Vibrational Spectroscopy

Some of the vibrational FTIR bands of the spectrum of ZnLos have previously been assigned and compared with the

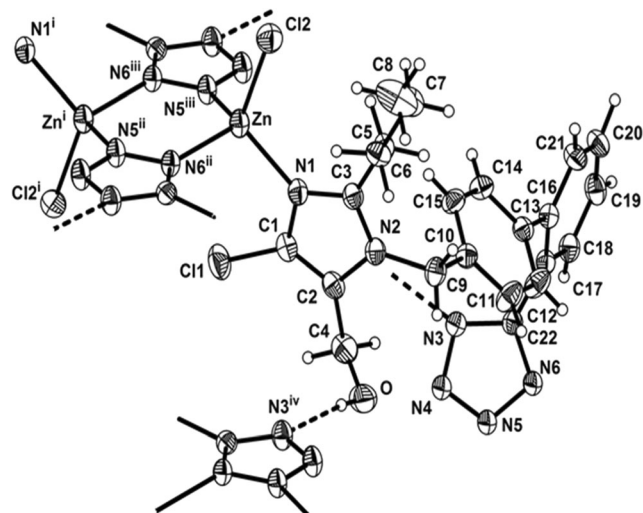


Fig. 2 Drawing of chlorolosartanatezinc(II) complex showing the labeling of the non-H atoms and their displacement ellipsoids at the 30% probability level. OH...N bonds are indicated by dashed lines. Symmetry operations: (i) $1-x, 1-y, 2-z$; (ii) $-1/2+x, 3/2-y, 1/2+z$; (iii) $3/2-x, -1/2+y, 3/2-z$; (iv) $3/2-x, 1/2+y, 3/2-z$

Table 2 Bond lengths [Å] and angles [°] around Zn(II) ion in chloro-losartan-zinc(II) complex

N(1)–Zn	2.016 (3)
Cl(2)–Zn	2.211 (1)
Zn–N(6)#1	2.034 (3)
Zn–N(5)#2	2.041 (3)
N(1)–Zn–N(6)#1	110.8 (1)
N(1)–Zn–N(5)#2	107.1 (1)
N(6)#1–Zn–N(5)#2	103.8 (1)
N(1)–Zn–Cl(2)	116.9 (1)
N(6)#1–Zn–Cl(2)	109.3 (1)
N(5)#2–Zn–Cl(2)	108.0 (1)

Symmetry transformations used to generate equivalent atoms:

(#1) $x - 1/2, -y + 3/2, z + 1/2$; (#2) $-x + 3/2, y - 1/2, -z + 3/2$

spectrum of protonated losartan (HLos) and losartan potassium salt (KLos) [9]. Herein, we have assigned the vibrational FTIR and Raman spectra of KLos and $[\text{Zn}(\text{Los})_2] \cdot 3\text{H}_2\text{O}$ by comparison with our computational studies on other sartans [29, 30]. According to the results shown in Table 3, the N–H stretching band (at ca. 3500 cm^{-1}) is absent due to the deprotonation of the losartan potassium salt and the O–H stretching bands of the ligand and of the water molecules of the complex are located in the $3380\text{--}3180 \text{ cm}^{-1}$ range. Small modifications are found in the bending COH and stretching CO (COH) modes upon coordination. The symmetric CN and CC aromatic stretching bands (ca. $1615\text{--}1524 \text{ cm}^{-1}$) show higher intensities in the Raman spectra, as expected. The infrared and Raman vibrational modes of the C–C bridge bond biphenyl of losartan (1260 and 1206 cm^{-1}) have been shifted in positions and show different intensities upon complexation. The main changes in the vibrational spectra of the complex are due to the modes of the tetrazole group (from 1100 to 954 cm^{-1}) indicating that the coordination of the zinc cation occurred through this anionic moiety of the ligand. The changes observed in the vibrational spectra of the OH modes may be indicative that this group is also involved in the coordination to the metal center.

The vibrational spectrum of the crystal $[\text{Zn}(\text{Los})\text{Cl}]$ showed some changes with respect to the spectrum powder complex $[\text{Zn}(\text{Los})_2] \cdot 3\text{H}_2\text{O}$. The OH stretching appeared as a very strong band, shifted to low energy because the H atom is bonded to the N atom of tetrazole (H bond, see Fig. 2). Bands related to the COH bending were also shifted (1154 cm^{-1}) with respect to the ligand and the spectrum of the powder complex. The coordination of the Zn ion to the imidazole group in this complex produced a shift of the bands assigned to νCN (1460 and 1426 cm^{-1}) to higher energies. The resolved structure of the complex showed the presence of a tetrazole bridge and then these vibrational modes must appear shifted with respect to the powder complex bands. In effect, the new band at 1032 and the 1013 cm^{-1} band that shifted to the blue, are indicative of a different coordination mode of the tetrazole group to the Zn ion.

Biological Studies

The $[\text{Zn}(\text{Los})_2] \cdot 3\text{H}_2\text{O}$ complex has been selected for the biological determinations due to its higher solubility. Considering previous reports that showed that the cytotoxic effects of ZnSO_4 were most likely due to the Zn ions rather than the sulfate ions and that ZnCl_2 exhibited pronounced cytotoxic effects, even stronger than those caused by Zn sulfate, we have selected the latter salt for the biological studies [31]. Stability studies have been performed measuring the variation of the ZnLos electronic absorption spectra and the molar conductivities with time. For the electronic absorption spectra measurements, the dissolution of the complex was performed in EtOH 96%. There was no observable variation in the electronic spectra of the ethanolic solution of the complex at least during 90 min (Fig. S1). The same behavior has been observed for DMSO solutions (data not shown). These results demonstrated that during the manipulation time of the samples for the biological determinations, a significant amount of the complex remained without decomposition. Conductivity measurements of 1-mM individual solutions of ZnSO_4 , losartan potassium salt in water, and ZnLos in DMSO, and a 0.5% DMSO- H_2O mixture were carried out at $25 \text{ }^\circ\text{C}$. The molar conductivity values for solutions of ZnSO_4 and the losartan potassium salt resulted 171 and $68 \text{ } \Omega^{-1} \text{ cm}^2/\text{mol}^{-1}$, respectively, typical for 2:2 and 1:1 electrolytes and similar to previous reported data [32, 33]. These values are practically unchanged up to 4 h (data not shown). The molar conductivity of the complex either in water or in a 0.5% DMSO- H_2O mixture (14 and $13 \text{ } \Omega^{-1} \text{ cm}^2/\text{mol}^{-1}$, respectively) is indicative of an undissociated neutral Zn(II) complex. This molar conductivity values remain unchanged up to 4 h (see Table 4). Hence, it has been determined using two experimental assays that the complex in solution stands without decomposition at least during the first 4 h of manipulation.

Behavior on Alkaline Phosphatase Activity

Alkaline phosphatase (ALP) is a homodimeric enzyme widely distributed and it has been isolated from eukaryotes as well as from prokaryotes. It hydrolyzes non-specifically phosphate monoesters at alkaline pH to produce inorganic phosphate and an alcohol. It is present in a number of tissues including liver, bone, intestine, and placenta. Serum ALP is of interest in the diagnosis of hepato and bone diseases. A considerable rise in ALP activity is produced in various types of malignant tumors and is used as a tumor marker [14] and also in different injuries such as brain and cerebrovascular diseases [34]. The inhibition of ALP has been related to the improvement of some diseases and for instance, the inhibitory effect of vanadate anion has directly been associated with the insulin-enhancing activity of vanadate complexes [35]. All highly purified alkaline phosphatases have proved to be Zn(II) metalloenzymes and this metal behaved as activator due to the saturation of Zn(II) binding

Table 3 Proposed assignments of the vibrational Raman (italics) and FTIR spectra of losartan potassium salt and the complex [Zn(Los)₂].3H₂O (ZnLos). Comparison with the FTIR spectrum of the single crystal [Zn(Los)Cl]. Wavenumber values in centimeters

Assignments	KLos	ZnLos	[Zn(Los)Cl]
ν O–H	3189 (s)	3376 (s)	3352 (vs) H bond
ν CH arom iph	3057 (sh)	3059 (m)	3064 (w)
	<i>3061 w</i>	<i>3070 w</i>	
ν CH arom oph	3033 (sh)	3028 (m)	3032 (w)
ν CH as CH ₃	2957 (s)	2955 (s)	2957 (s)
	<i>2971 m</i>	<i>2965 m</i>	
ν CHs CH ₃	2930 (vs)	2930 (s)	2936 (s)
ν CH s CH ₂	2871 (m)	2868 (m)	2871 (m)
ν CN	1613 (vw)	1603 (w)	1596 (w)
	<i>1614 vs, 1606 s</i>	<i>1615 vs, 1605 s,</i>	
ν CC	1579 (m)	1577 (w)	1560 (w)
	<i>1578 m</i>	<i>1582 m, 1567 sh</i>	
ν CN ip arom + ν CC	1527 (vw)	1527 (sh)	
	<i>1524 s</i>	<i>1527 m</i>	
ν CC	1507 (sh)	1509 (sh)	1508 (sh)
	<i>1509 m, 1502 m</i>	<i>1509 m</i>	
ν CC + δ CCH ip + ν CN	1497 (m)	1494 (sh)	1480 (sh)
	<i>1498 m</i>	<i>1498 m</i>	
δ CCH ip + ν CN	1460 (m), 1422 (s)	1460 (vs), 1426 (m)	1466 (vs), 1435 (sh)
	<i>1462 vw, 1427 w</i>	<i>1463 w, 1432 w, 1425 w</i>	
ν CC + δ CCH ip	1408 (m), 1380 (m)	1409 (m), 1382 (m)	1410 (sh)
CH ₂ wag	1357 (m)	1356 (m)	1363 (m)
δ COH + δ CCH	1341 (m)	1351 (sh)	1340 (sh)
CH ₂ wag + CH ₂ rock	1309 (w)	1310 (w)	1310 (sh)
	<i>1294 s</i>	<i>1298 s</i>	
ν C–C bridge bond biphenyl	1260 (s), 1237 (sh)	1255 (s)	1256 (m)
	<i>1261 vw</i>	<i>1253 m</i>	
ν NN + ν C–C bridge bond biphenyl	1206 (m)	1222 (m)	
	<i>1208 m</i>		
ν CO (COH) + δ CCH arom, CH ₂ rock and wag	1187 (m)	1190 (sh)	1154 (m)
	<i>1187 m</i>	<i>1193 m</i>	
ν NN	1132 (m), 1112 (m)	1105 (w)	
CH ₂ rock + δ CCH ip arom	1107 (m)	1092 (w)	1097 (m)
ν NN + δ CCH ip arom + ring breath	1074 (m)	1074 (w), 1025 (sh)	1032 (m)
δ NNN + ν NN	999 (s)	1007 (s)	1013 (m)
	<i>1013 s</i>	<i>1010 w</i>	
δ CCH op arom + CH ₂ twist	954 (sh), 933 (m)	954 (w) 935 (w)	954 (w)
δ CCH op arom	885 (w), 840 (m)	882 (w), 825 (m)	887 (vw), 829 (m)
δ CCH op arom, ν C–Cl	762 (m)	762 (m)	762 (m)

vs very strong, s strong, m medium, w weak, sh shoulder, vw very weak, ip in plane, op out of plane, iph in phase, oph out of phase, arom aromatic ring

sites. Alkaline phosphatase from bovine intestinal mucosa is an homodimeric metalloenzyme, containing in each active site one Mg ion (for structural stabilization) and two Zn ions involved in catalysis and a novel fourth metal site is occupied by Ca(II). The addition of Zn increase the enzymatic activity but an excess of Zn could replace Mg at binding sites in the ALP hence producing an inhibitory effect [36]. The effects of the

compounds on ALP activity are shown in Fig. 3. Zn ion produced enzymatic activation up to a concentration of 0.5 mM. Losartan potassium salt showed low inhibitory effect that can be correlated to the chelating ability of losartan to the active sites of the enzyme. On the contrary, the ZnLos complex barely enhanced the activity of ALP, modulating the activating action of the Zn(II) ions.

Table 4 Molar conductance ($\Omega^{-1}\text{cm}^2\text{mol}^{-1}$) of solutions of ZnLos

<i>t</i> (min)	ZnLos ^a	ZnLos ^b
5	14	12
10	12	15
15	14	13
20	13	15
30	14	13
60	14	15
120	13	14
180	12	14
240	14	14

^a DMSO^b 0.5% DMSO/H₂O

Behavior on Acid Phosphatase Activity

Acid phosphatases are ubiquitous and abundant enzymes in plants, animals, fungi, and bacteria. Their action includes production, transport, and recycling inorganic phosphate which is crucial for cellular metabolism and bioenergetics. Intracellular and secreted AcPs are believed to play a major role in inorganic phosphate scavenging and the utilization and turnover of inorganic phosphate-rich sources occurring in either animal lysosomes or plant vacuoles [37]. In mammals, a role of AcPs is ascribed to iron transport (non-enzymatic process), bone resorption, and generation of reactive oxygen species (ROS) as an immune response. AcPs are abundantly expressed in osteoclasts, activated macrophages (in which the enzyme may play a role in the immune defense system increasing ROS production) and dendritic cells. A variety of biological roles have been proposed for plant AcPs due to its bifunctionality (hydrolysis

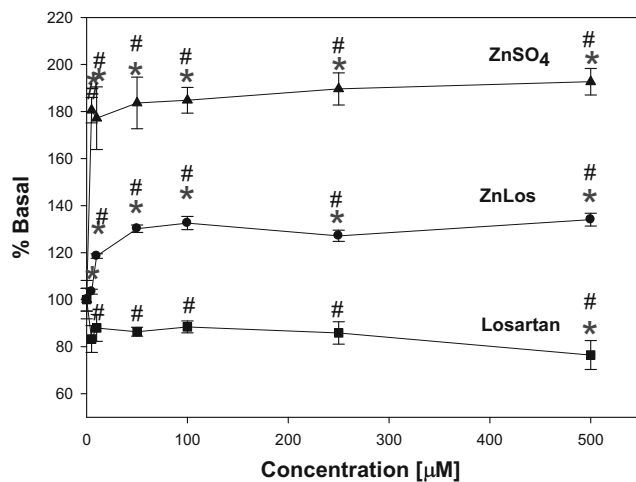


Fig. 3 Effect of ZnLos (circles), losartan (squares), and ZnSO₄ (triangles) on ALP activity from bovine intestinal mucose. The results are expressed as the percentage of the basal level and represent the mean \pm SEM ($n = 9$). Asterisk indicates significant differences versus basal $p < 0.05$. Pound sign indicates significant differences at the same concentration between ZnLos, losartan, and Zn, $p < 0.05$

and peroxidation). The major function of these enzymes is the mobilization of inorganic phosphates from organophosphates in the soil and the participation in phosphate metabolism [38]. AcP from potato is a nonspecific phosphomonoesterase with a Fe²⁺/Fe³⁺ catalytic site together with the co-catalytic sites of Mn²⁺, Zn²⁺, and trace copper [39]. The enzyme displayed a pH optimum of 5.8, was activated by Mg²⁺, and was potently inhibited by molybdate, vanadate, and Zn²⁺ [15].

From Fig. 4, it can be seen that while losartan exerted low effects on AcP, the Zn ion inhibited the enzymatic activity in a dose-response manner and the ZnLos complex behaved like the metal at concentrations higher than 75 μM . A pattern of low and high activity has been observed in bony tissues of rats, as well as a pattern of low alkaline phosphatase activity during acid phosphatase activity peaks and vice versa [40]. Phosphoregulation is involved in many biological events and often occurs as a network-like cascade, in which activity of one phosphatase or kinase is dependent on the upstream activity of another. The same concerted mechanism has been displayed by the Zn ion and the ZnLos complex at the tested concentrations: a decrease of the AcP activity has been associated with an increase in the ALP activity.

Biological Effects on Human Lung A549 Cancer Cell Line

MTT Assay

The cytotoxic effects of ZnSO₄, losartan, and ZnLos complex on A549 cell line were determined by the MTT assay. The viability of the normal human lung fibroblasts cell line MRC-5 incubated with the different compounds has also been

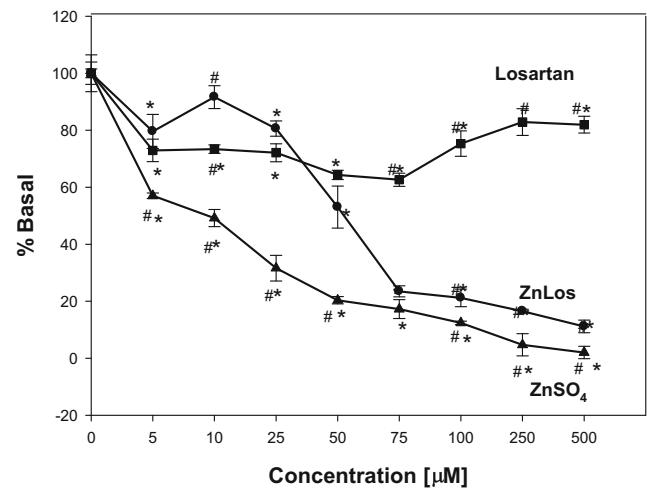


Fig. 4 Effect of ZnLos (circles), losartan (squares), and ZnSO₄ (triangles) on AcP activity from potato. The results are expressed as the percentage of the basal level and represent the mean \pm SEM ($n = 9$). Asterisk indicate significant differences versus basal $p < 0.05$. Pound sign indicate significant differences at the same concentration between ZnLos, Los, and Zn, $p < 0.05$

studied. Cancer cells were treated with different concentration (0–500 μM) for 24 h. As shown in Fig. 5, no cytotoxicity was observed in losartan up to 250 μM concentration. A similar low effect of this antihypertensive drug at high concentrations has been measured for leukemic cell lines [41] but reports on A549 lung cancer cells (72-h incubation) were somewhat different [42]. Cell viability decreased upon cellular incubation with ZnSO_4 from 100 μM , as has previously been determined [43]. The complex ZnLos declined cell proliferation in a dose-dependent manner and showed a significantly decrease from 50 μM .

The cytotoxic effect of the compounds has been evaluated in a human normal lung fibroblasts MRC-5 cell line. It can be seen (Fig. 6) that the compounds did not exhibit significant cytotoxic activities up to 150- μM concentration. This behavior has also been reported for losartan in human normal lung fibroblasts, WI-38 [42]. From Fig. 6, a cytotoxic effect of an excess of Zn(II) ions at concentrations higher than 200 μM (see Section “ROS Generation”) in this normal cell line can be seen. Then, it could be demonstrated that losartan complexation attenuates the toxic effect of Zn at elevated concentrations.

ROS Generation

Like an essential element, the excess of zinc is toxic, inducing apoptosis in cell lines that involve oxidative stress production [44]. Cancer cells display an intrinsic oxidative stress higher than normal cells. Hence, the exposure to ROS generating compounds will cause more injury in cancer cell lines due to a decrease of the antioxidant defenses. Zinc ions are able to

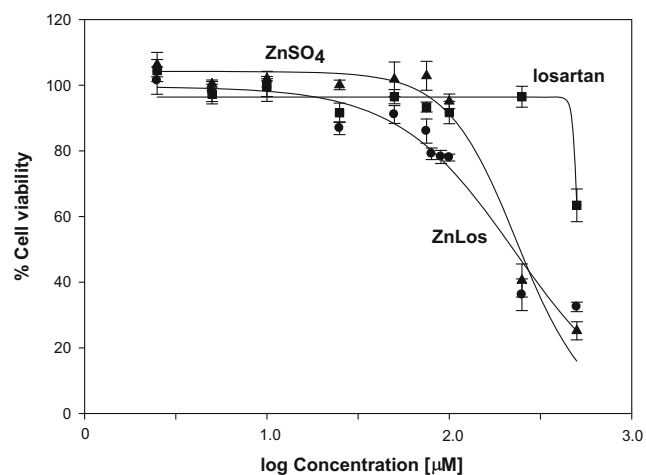


Fig. 5 Effect of ZnLos (circles), losartan (squares), and ZnSO_4 (triangles) on A549 cellular viability. The cell line was incubated with different concentrations (0–500 μM) of the compounds for 24 h. Each point represents mean \pm SD of three independent experiments and it express the percentage of the basal level. Asterisk indicate significant differences versus basal $p < 0.05$. Pound sign indicates significant differences at the same concentration between ZnLos, losartan, and ZnSO_4 , $p < 0.05$

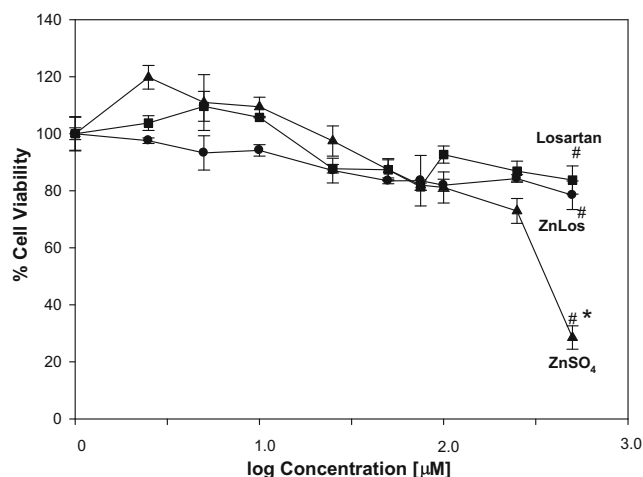


Fig. 6 Effect of ZnLos (circles), Los (squares), and ZnSO_4 (triangles) on human normal lung fibroblasts MRC-5 cell proliferation in dose-dependent manner. The cell line was incubated with different concentrations (0–500 μM) of the compounds for 24 h. Each point represents mean \pm SD of three independent experiments and it express the percentage of the basal level. Asterisk indicates significant differences versus basal $p < 0.05$. Pound sign indicates significant differences at the same concentration between $[\text{Zn}(\text{Los})_2] \cdot 3\text{H}_2\text{O}$, Los, and Zn, $p < 0.05$

induce oxidative stress in cancer cells by different molecular mechanisms. The enhancement of ROS production could be generated by the induction of mitochondrial respiration impairment, the inhibition of glutathione reductase activity or the inhibition of the lipoamide dehydrogenase multienzyme complex (LADH), which has a role in the preservation of the reducing environment of mitochondria [45]. Acidosis, an increase of ROS generation in several tumor cells and stimulation of apoptosis by zinc exposure has been reported [9]. ROS generation was detected and quantified in response of the incubation of the A549 cells with ZnSO_4 , losartan and ZnLos for 24 h (Fig. 7). Cells treated with increasing concentrations of ZnSO_4 (from 100 μM) showed an increase in the oxidative stress, as expected in comparison with reported data in A549 cell line [31]. Upon incubation with increasing doses of ZnLos and losartan a significant increase and a decrease in oxidative stress, respectively, has been detected. These results suggested that the production of ROS plays a key role in the ZnSO_4 and ZnLos-induced apoptosis (see below) and subsequent cell death.

GSH Content and GSH/GSSG Ratio

To further analyze the involvement of ROS in ZnLos-induced cell death, the levels of reduced glutathione (GSH) and the GSH/GSSG ratio was estimated in the cells after ZnLos treatment for 24 h (Fig. 8). The antioxidant cellular levels were also measured for losartan and Zn(II) ions. A significant decrease of cellular GSH content after ZnLos treatment for 24 h was found. A concomitant depletion in the intracellular GSH

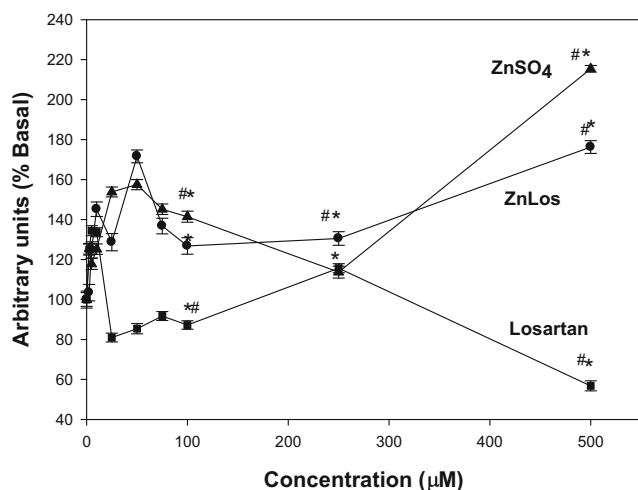


Fig. 7 Effect of 0–500 μM losartan, ZnSO_4 , and ZnLos on dihydrorhodamine 123 (DHR) oxidation to rhodamine 123. A549 cells were incubated at 37 $^\circ\text{C}$ in the presence of 10 μM DHR for 30 min. The values are expressed as the percentage of the control level and represent the mean \pm SEM. Asterisk indicates significant values in comparison with the control level ($p < 0.05$)

levels and the GSH/GSSG ratio has been observed with the enhancement in ROS levels. Besides, GSH levels and GSH/GSSG ratio increased at low ZnSO_4 concentrations reaching maximum at ZnSO_4 concentration 25 μM corresponding with the hypoxia (low oxygen stress) state of A549 cells and decreased at higher concentrations. This decrease has previously been reported (up to 100 μM) [46] and explained on the basis that zinc transporters played an important role in the resistance to high concentrations of extracellular zinc. Losartan showed some decay of GSH content and had no changes in GSH/GSSG ratio. Then, it can be demonstrated that increased ROS production followed by mitochondrial GSH depletion represented a crucial event, which irreversibly produced cell death.

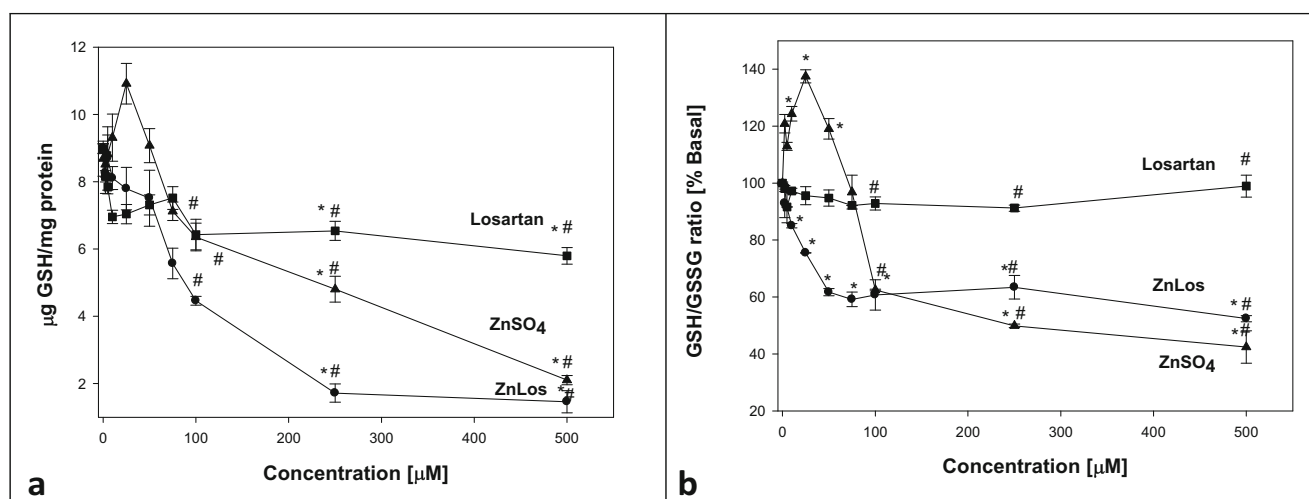


Fig. 8. Microgram of glutathione (GSH) per milligram of protein (**a**) and GSH/GSSG ratio (**b**) as percentage of the basal level in A549 cells after treatment with 0–500 μM ZnLos (circles), losartan (squares), and ZnSO_4 (triangles) for 24 h. Each point represents mean \pm SD of three

TUNEL Assay

A sub-cytotoxic concentration of 25 and 100 μM have been determined for ZnLos and ZnSO_4 , respectively. Therefore, 500 μM concentration of each compound was used for further analysis. To determine the mechanisms of cell death, the generation of apoptotic cells by the action of the compounds on the A549 cell line has been determined. Despite that exposure to exogenous zinc resulted in increased apoptosis, growth inhibition, and altered oxidative stress in cancer cells [9], from Fig. 9a, it can be seen that ZnLos and losartan induced a significant increment of the apoptotic index (AI) in A549 cells ($p > 0.05$). However, the apoptotic induced effect of ZnLos was double higher than the noticed for losartan (Fig. 9b). It can then be concluded that the decrease in cell viability could be achieved by a programmed cellular death or apoptosis and that both ROS generation and GSH depletion could act as regulators.

Immunocytochemical Staining

The morphological changes caused by incubation of the cells with the different compounds are shown in Fig. 10. Cells treated with ZnSO_4 and ZnLos became round and the volume shrank. Apoptotic characteristics such as apoptotic bodies, agglutination, and margination of chromatin and cytoplasm vacuolization could be seen.

Apoptosis is modulated by antiapoptotic and proapoptotic effectors, which involves a large number of proteins. The proapoptotic and antiapoptotic members of the Bcl-2 family regulate programmed cell death and are targets of anticancer therapy [47]. The cytosolic proapoptotic BAX protein modified its conformation when initiation of apoptotic signaling

independent experiments. Asterisk indicates significant differences versus basal $p < 0.05$. Pound sign indicates significant differences at the same concentration between ZnLos, losartan, and Zn, $p < 0.05$

and becomes mitochondrial membrane-associated, producing the opening of the mitochondrial voltage-dependent anion channel. This process produced the loss in membrane potential and the release of cytochrome-c and caspase-3 activation. From Fig. 10, it can be seen that BAX and Caspase-3 protein expression were significantly higher in cells treated with 500 μ M ZnSO₄ and ZnLos than for losartan at the same concentration.

Then, it can be seen that the antiapoptotic Bcl-XL protein was significantly higher in cells treated with losartan and was lower in cells treated ZnSO₄ and ZnLos. The apoptogenic effect of elevated concentration of Zn, associated with increased levels of BAX or decreased Bcl-XL has also been observed in prostate cancer cells [9, 48].

Western Blotting

The ratio of proapoptotic proteins of Bcl2 family to antiapoptotic members that determines whether a cell

responds to a programmed cell death stimulus has also been examined using Western blotting. The ratio between BAX and Bcl-XL that determines whether cells undergo apoptosis correlated well with the immunohistochemical expression of the proteins. This ratio was found to be significantly higher in A549 cells exposed to ZnLos than cells treated with ZnSO₄. Losartan treatment caused low BAX/ Bcl-XL ratio. (Fig. 11).

The sequence of biochemical events occurring in human lung A549 cancer cells after modulation of the cellular redox state has been determined. The decline in cellular GSH, in response to ZnLos treatment, coincided with the induction of mediators of apoptotic signaling including mitochondrial BAX release and caspase-3 activation and an increase of the BAX/Bcl-XL ratio.

AO/EtBr Staining Assays

Because TUNEL assay fails to discriminate apoptotic from necrotic cells, AO/EtBr staining assays were performed to

Fig. 9 **a** Representative photomicrographs of the TUNEL assay corresponding to negative control (DMSO), positive control (recombinant DNase), losartan, ZnSO₄, and ZnLos. Original magnification $\times 40$. **b** Bars represent percentages of TUNEL-positive nuclei. Values are mean \pm SEM. Pound sign indicates significant differences at the same concentration between ZnLos, losartan, and ZnSO₄; $p < 0.05$

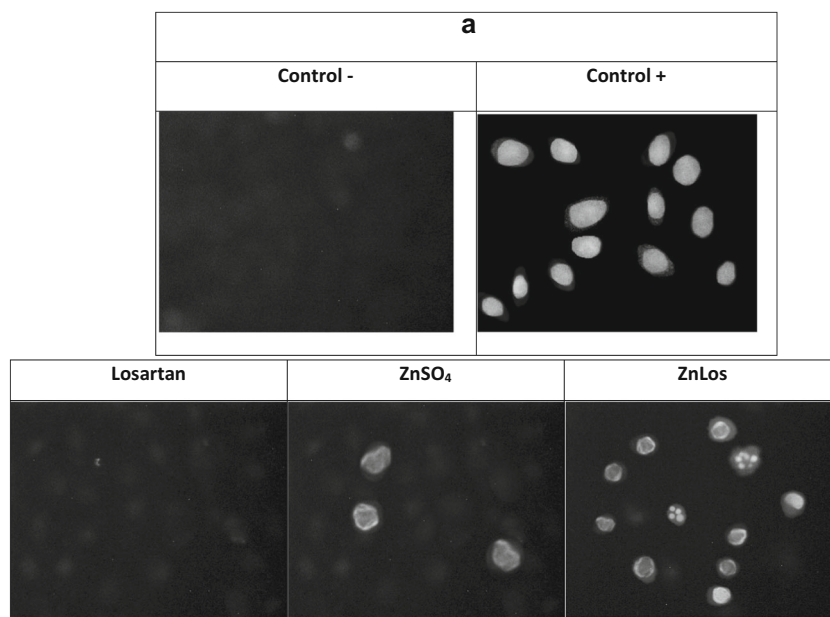
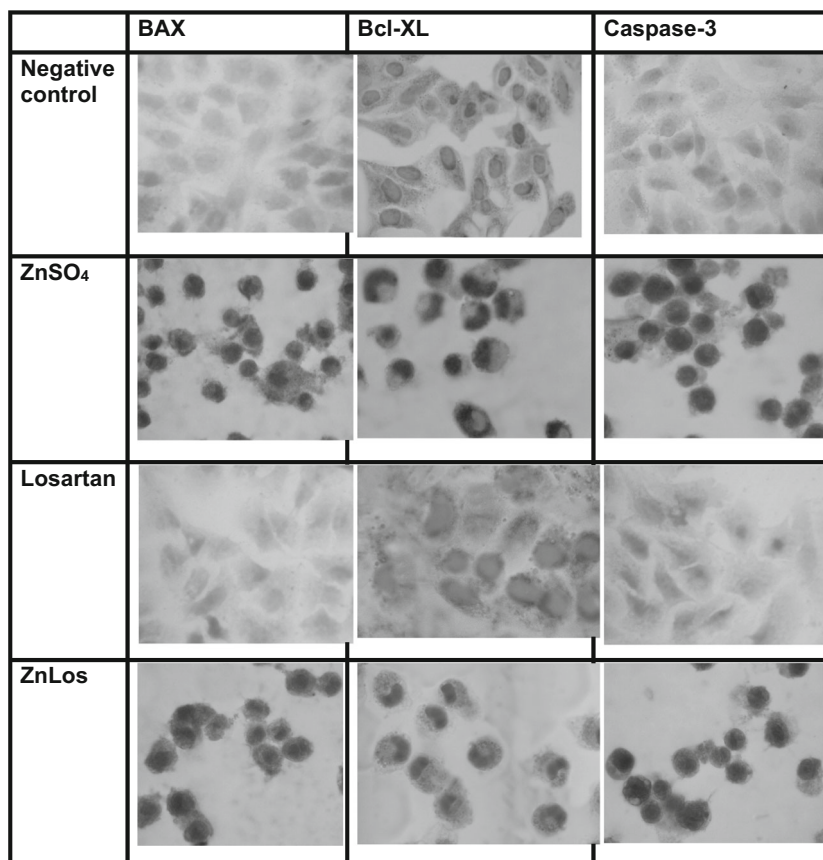


Fig. 10 Immunocytochemical staining presenting BAX, Bcl-XL, and Caspase-3 expression in cells treated with 500 μ M losartan, ZnSO₄, and ZnLos. Negative control: DMSO. One representative immunocytochemical analysis shown per protein. Original magnification \times 40



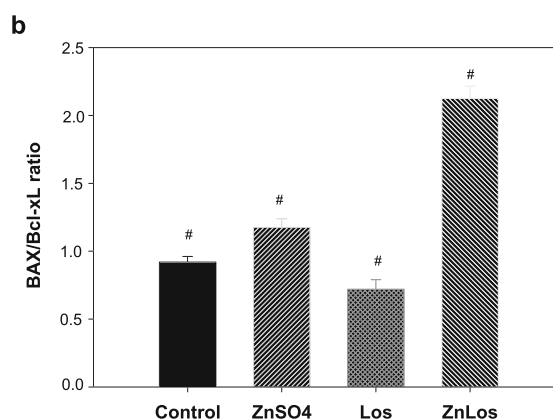
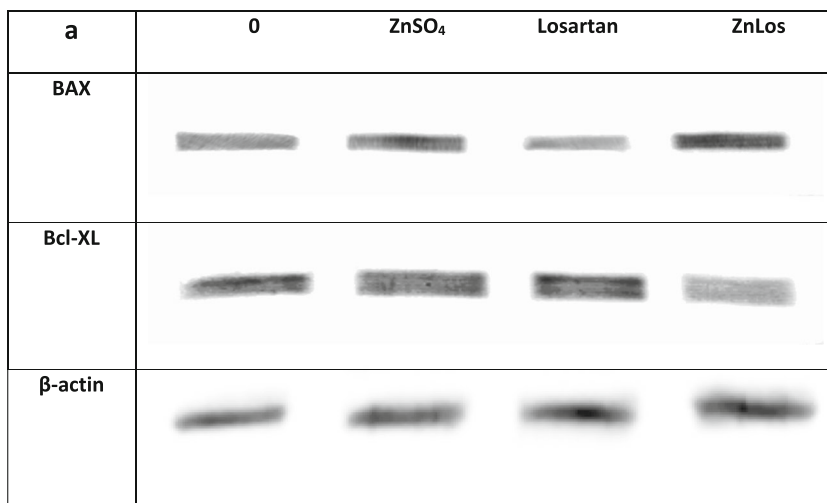
detect living, apoptotic, and necrotic cells after treatment with Los, ZnSO₄, and ZnLos. Early apoptotic cells show condensed nuclei and appear bright green in color and late apoptotic cells appear in red color with condensed and fragmented nuclei. After staining with AO/EtBr, control untreated cells appeared green in color with intact nuclei. Cells treated with ZnLos and ZnSO₄ revealed morphological changes associated with apoptosis, consistently with TUNEL observations: bright green nuclei with condensed chromatin, apoptotic bodies, shrunken, and margination of nuclei. However, cells treated with ZnSO₄ have shown more cells with normal morphological aspect. In contrast, losartan treatment showed normal and large nucleus with normal morphology like the untreated cells. In necrotic cells, EtBr penetrated into the membranes of dead cells and stains their nuclei which appear red. From the data of Fig. S2, it was clear that with the addition of increasing concentrations of the compounds no changes associated with necrosis were observed. Therefore, necrotic effects could be discarded even at concentrations of 500 μ M (higher than sub-cytotoxic doses).

Discussion

We have previously determined that the antihypertensive drug losartan did not displayed anticancer effects in a bone cancer

cell line (UMR106) at the maximum tested concentration value (500 μ M) but copper(II) complexation enhanced the cell killing effect of the ligand [49]. Then, we could determine that the introduction of a structural modification of losartan by metal complexation enhanced its antiproliferative action. On the other hand, we have performed a structural modification of azilsartan, a modern angiotensin II receptor antagonist by Zn(II) complexation, considering that some studies suggested that the biometal Zn displayed anticancer effects. The complex ZnAzil also produced a significant decrease in the viability of the A549 lung cancer cell line in comparison to the antihypertensive drug through a mitochondrial apoptotic pathway [11]. We herein report the biological behavior of a complex formed between losartan and Zn(II). Like Cu(II) ions, the Zn(II) ions are also able to modify the structure and the anticancer properties of losartan, measured in the lung cancer cell line A549. The proposed mechanism for the anticancer effect of the ZnLos complex is shown in Fig. 12. It is well-known that ROS may act as important inducers of the intrinsic mitochondrial apoptotic pathway. The present study demonstrated that ZnLos complex (500 μ M) clearly caused GSH depletion and a shift in GSSG levels in A549 cell cultures implying an imbalance in redox metabolism. This event was concomitant with 40% of apoptotic index enhancement determined by TUNEL assay. Additionally, the upregulation of BAX levels with the simultaneous downregulation of Bcl-XL in A549

Fig. 11 BAX and Bcl-xL expression in A549 cells. **a** Representative Immunoblot images corresponding to cultures treated with 500 μ M ZnSO₄, losartan, ZnLos, and DMSO (negative control). Immunoblottings were performed by triplicate from a single sample of three independent experiences. The β actin was used as an internal loading control. **b** BAX/Bcl-XL ratio. Protein levels were analyzed by densitometry using Scion Image Software (NIH USA). Data were normalized to beta-actin. Pound sign indicates significant differences between ZnSO₄, losartan, and ZnLos, $p < 0.05$



cells treated with the aforementioned concentration of ZnLos complex, suggests that the changes in the BAX/Bcl-XL ratio, could allow BAX to be available to signal apoptosis through the intrinsic apoptotic pathway. Thus, the mitochondrial pores in the outer membrane with the depolarization of the transmembrane potential trigger the release of the proapoptotic

factor BAX and the cytochrome-c to cytoplasm, which lead to the caspase-3 activation and the subsequent DNA cleavage.

Table 5 displayed data of cell survivals and oxidative stress measured after cellular incubation with ZnLos and ZnAzil complexes. As it can be seen, ZnAzil complex produces high levels of ROS at each tested concentration thereby causing

Fig. 12 Diagram of the proposed mechanism for the anticancer effect of the ZnLos complex

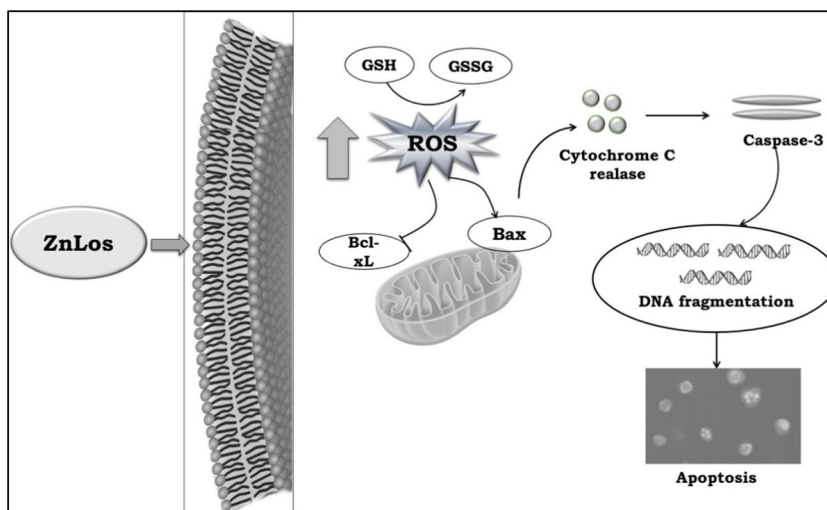


Table 5 Comparison of the effects of the Zn(II) complexes of losartan (ZnLos) and azilsartan (ZnAzil) on the percentage of cell survival and ROS and GSH/GSSG cellular levels on A549 lung cancer cell line

	ZnLos			ZnAzil ^a	
	100	250	500	100	250
Concentration, μM	100	250	500	100	250
Cell survival, % basal	78	36	32	59	21
ROS, % basal	126	130	176	189	207
GSH/GSSG	61	63	52	55	38

^a From [8]

oxidation of the main cellular antioxidant GSH. The depletion on the glutathione to oxidized glutathione ratio that potentially diminished the antioxidant defenses follows the same trend. As a consequence, although both complexes exerted anticancer effects, A549 cell line survival resulted lower upon ZnAzil treatment. Even though TUNEL, immunocytochemical staining and Western blotting assays were performed at different concentrations for ZnLos and Zn Azil, it has been demonstrated that both compounds exerted their anticancer effects by programmed cell death or apoptosis through the mitochondrial pathway, regulated by the Bcl-2 family of proteins.

Conclusions

Due to the flexible coordination ability and characteristic coordination behavior, such as folded conformation of the tetrazole and imidazole N atoms, two different coordination modes for Zn(II) ion coordination to losartan were obtained, working at different experimental conditions. Three-dimensional aggregation is achieved with the tetrazole groups bridging the Zn(II) ions and by the coordination of the remote imidazole groups of losartanate to the metal center giving a metal to ligand (1:1) stoichiometry, [Zn(Los)Cl]. A previous reported complex with two losartanate groups coordinated to the Zn(II) metal center has also been prepared as a powder. Structural determinations for this known complex, [Zn(Los)₂].3H₂O (ZnLos), could not be performed because attempts to obtain single crystals failed. Both compounds were characterized by vibrational and diffuse reflectance spectroscopies but the latter compound has been selected for the biological tests because of its high solubility.

The complex ZnLos and the Zn(II) ions showed a concerted mechanism for the interaction with phosphatases at the tested concentrations: a decrease of the AcP activity has been associated with an increase in the ALP activity. A weak effect of losartan on phosphatases inhibition has been determined. The present study showed that ZnLos could induce oxidative stress correlating with cytotoxicity in the human alveolar carcinoma cell line A549. The programmed cell death involved a significant increase of ROS generation upon incubation with

the ZnLos complex followed by depletion of GSH that induces apoptosis through the intrinsic pathway and no necrosis has been detected. The present report about chemical and anticancer effect of ZnLos on A549 cells, contribute to new knowledge about the potential use complex for inducing the mitochondrial apoptotic pathway in lung adenocarcinoma treatments. According to our measurements, ZnSO₄ produced lower levels of ROS and higher levels of the natural intracellular antioxidant system, GSH up to 50 μM concentrations, and then it did not show cytotoxic effects on the cancer A549 cell line. Then, supplementation of ZnLos complex instead of a ZnSO₄ salt in hypertensive patients could modulate the anticancer effect of the biometal at low concentrations. However, further molecular studies are required to know the benefits of the treatment with ZnLosartan as an antitumor therapeutic agent.

Acknowledgements This work was supported by UNLP, CONICET (PIP 0611), CICPBA (PICyT 813/13), and ANPCyT (PICT-2016-1814, PME06 2804 and PICT06 2315), Argentina. VRM is a fellowship holder from ANPCyT. EGF, LGN, GAE, and OEP are research fellows of CONICET. PAMW is a research fellow of CICPBA, Argentina.

References

1. Ferlay J, Shin HR, Bray F, Forman D, Mathers C, Parkin DM (2010) Estimates of worldwide burden of cancer in 2008: GLOBOCAN 2008. *Int J Cancer* 127:2893–2917. <https://doi.org/10.1002/ijc.25516>
2. Timmermans PB, Duncia JV, Carini DJ, Chiu AT, Wong PC, Wexler RR, Smith RD (1995) Discovery of losartan, the first angiotensin II receptor antagonist. *J Hum Hypertens* 5:S3–S18
3. Li J, Chen L, Yu P, Liu B, Zhu J, Yang Y (2014) Telmisartan exerts anti-tumor effects by activating peroxisome proliferator-activated receptor- γ in human lung adenocarcinoma A549 cells. *Molecules* 19:2862–2876. <https://doi.org/10.3390/molecules19032862>
4. Gallagher PE, Tallant EA (2004) Inhibition of human lung cancer cell growth by angiotensin-(1-7). *Carcinogenesis* 25:2045–2052. <https://doi.org/10.1093/carcin/bgh236>
5. Islas MS, Luengo A, Franca CA, Grier Merino M, Calleros L, Rodríguez-Puyol M, Lezama L, Ferrer EG, Williams PAM (2016) Experimental and DFT characterization, antioxidant and anticancer activities of a Cu(II)-irbesartan complex: structure-antihypertensive activity relationships in Cu(II)-sartan complexes. *J Biol Inorg Chem* 21:851–863. <https://doi.org/10.1007/s00775-016-1384-5>
6. Ho E (2004) Zinc deficiency, DNA damage and cancer risk. *J Nutr Biochem* 10:572–578
7. Singh KP, Zaidi SI, Raisuddin S, Saxena AK, Murthy RC, Ray PK (1992) Effect of zinc on immune functions and host resistance against infection and tumor challenge. *Immunopharmacol Immunotoxicol* 14:813–840
8. Prasad AS, Kucuk O (2002) Zinc in cancer prevention. *Cancer Metastasis Rev* 21:291–295. <https://doi.org/10.1023/A:1021215111729>
9. Kocdor H, Ates H, Aydin S, Cehreli R, Soyarat F, Kemanli P, Harmanci D, Cengiz H, Kocdor MA (2015) Zinc supplementation induces apoptosis and enhances antitumor efficacy of docetaxel in non-small-cell lung cancer. *Dovepress* 9:3899–3909. <https://doi.org/10.2147/DDDT.S87662>

10. Braun LA, Rosenfeldt F (2013) Pharmaco-nutrient interactions—a systematic review of zinc and antihypertensive therapy. *Int J Clin Pract* 67:717–725. <https://doi.org/10.1111/ijcp.12040>
11. Martínez VR, Aguirre MV, Todaro JS, Piro OE, Echeverría GA, Ferrer EG, Williams PAM (2018) Azilsartan and its Zn(II) complex. Synthesis, anticancer mechanisms of action and binding to bovine serum albumin. *Toxicol In Vitro* 48:205–220. <https://doi.org/10.1016/j.tiv.2018.01.009>
12. Teixeira JA, Siqueira AB (2016) Thermal and spectroscopic characterization, antioxidant evaluation and pyrolysis of losartan with some bivalent metals. *J Anal Appl Pyrol* 117:17–24. <https://doi.org/10.1016/j.jaap.2015.12.023>
13. Lachowicz JI, Nurchi VM, Crisponi G, Jaraquemada-Pelaez MG, Caltagirone C, Peana M, Zoroddu MA, Szweczek Z, Cooper GJS (2017) Complex formation equilibria of Cu(2+) and Zn(2+) with irbesartan and losartan. *Eur J Pharm Sci* 97:158–169. <https://doi.org/10.1016/j.ejps.2016.11.010>
14. Fishman WH (1987) Alkaline phosphatase: an overview. *Clin Biochem* 20:387–392. <https://doi.org/10.1007/2Fs12291-013-0408-y>
15. Bozzo GG, Raghothama KG, Plaxton WC (2004) Structural and kinetic properties of a novel purple acid phosphatase from phosphate-starved tomato (*Lycopersicon esculentum*) cell cultures. *Biochem J* 377:419–428. <https://doi.org/10.1042/BJ20030947>
16. CrysAlisPro, Oxford Diffraction Ltd., version 1.171.33.48 (release 15–09-2009 CrysAlis171.NET)
17. Sheldrick GM (2008) A short history of SHELX. *Acta Crystallogr A* 64:112–122. <https://doi.org/10.1107/S0108767307043930>
18. Ferrer EG, Salinas MV, Correa MJ, Naso L, Barrio DA, Etcheverry SB, Lezama L, Rojo T, Williams PAM (2006) Synthesis, characterization, antitumoral and osteogenic activities of quercetin vanadyl (IV) complexes. *J Biol Inorg Chem* 11:791–801. <https://doi.org/10.1007/s00775-006-0122-9>
19. Blum U, Schwedt G (1998) Inhibition behavior of acid phosphatase, phosphodiesterase I and adenosine deaminase as tools for trace metal analysis and speciation. *Anal Chim Acta* 360:101–108. [https://doi.org/10.1016/S0003-2670\(97\)00717-4](https://doi.org/10.1016/S0003-2670(97)00717-4)
20. Glaysher S, Cree I (2011) Isolation and culture of colon cancer cells and cell lines. *Meth Mol Biol* 731:135–140. https://doi.org/10.1007/978-1-61779-080-5_12
21. Qin Y, Lu M, Gong X (2008) Dihydrohodamine 123 superior to 2, 7-dichlorodihydrofluorescein diacetate and dihydrohodamine 6G in detecting intracellular hydrogen peroxide tumor cells. *Cell Biol Int* 32:224–228. <https://doi.org/10.1016/j.cellbi.2007.08.028>
22. Bradford M (1976) A rapid and sensitive method for the quantitation of microgram quantities of protein utilizing the principle of protein-dye binding. *Anal Biochem* 72:249–254. [https://doi.org/10.1016/0003-2697\(76\)90527-3](https://doi.org/10.1016/0003-2697(76)90527-3)
23. Hissin PJ, Hilf R (1976) A fluorometric method for determination of oxidized and reduced glutathione in tissues. *Anal Biochem* 74:214–226. [https://doi.org/10.1016/0003-2697\(76\)90326-2](https://doi.org/10.1016/0003-2697(76)90326-2)
24. Negoescu A, Guillemet C, Lorimier P, Brambilla E, Labat-Moleur F (1998) Importance of DNA fragmentation in apoptosis with regard to TUNEL specificity. *Biomed Pharmacother* 52:252–258. [https://doi.org/10.1016/S0753-3322\(98\)80010-3](https://doi.org/10.1016/S0753-3322(98)80010-3)
25. Liu QY, Stein C (1997) Taxol and estramustine-induced modulation of human prostate cancer cell apoptosis via alteration in bcl-xL and bak expression. *Clin Cancer Res* 3(11):2039–2046
26. Aguirre MV, Juaristi JA, Alvarez MA, Brandan NC (2005) Characteristics of in vivo murine erythropoietic response to sodium orthovanadate. *Chem Biol Interact* 156:55–68. <https://doi.org/10.1016/j.cbi.2005.07.003>
27. Ribble D, Goldstein NB, Norris DA, Shellman YG (2005) A simple technique for quantifying apoptosis in 96-well plates. *BMC Biotechnol* 5:1–7. <https://doi.org/10.1186/1472-6750-5-12>
28. Farrugia LJ (1997) ORTEP3 for windows. *J Appl Crystallogr* 30:565
29. Franca CA, Etcheverry SB, Pis Diez R, Williams PAM (2009) Irbesartan: FTIR and Raman spectra. Density functional study on vibrational and NMR spectra. *J Raman Spectrosc* 40:1296–1300. <https://doi.org/10.1002/jrs.2282>
30. Islas MS, Franca CA, Etcheverry SB, Ferrer EG, Williams PAM (2012) Computational study and spectroscopic investigations of antihypertensive drugs. *Vibrat Spectrosc* 62:143–151. <https://doi.org/10.1016/j.vibspec.2012.04.009>
31. Kőnczöl M, Goldenberg E, Ebeling S, Schäfer B, Garcia-Käuffer M, Gminski R, Grobety B, Rothen-Rutishauser B, Merfort I, Gieré R, Mersch-Sundermann V (2012) Cytotoxicity and genotoxicity of size-fractionated iron oxide (magnetite) in A549 human lung epithelial cells: role of ROS, JNK, and NF-κB. *Chem Res Toxicol* 25:2687–2703. <https://doi.org/10.1021/tx200051s>
32. Vink H (1994) Electrolytic conductivity of mixed electrolyte solutions. *Ber Bunsenges Phys Chem* 98:1039–1045
33. de Oliveira RP, Felix FS, Angnes L (2012) A simple and precise conductometric method for the determination of losartan in pharmaceutical products. *Cent Eur J Chem* 10:1842–1849. <https://doi.org/10.2478/s11532-012-0110-6>
34. Kellet KAB, Williams J, Vardy ERLC, Smith AD, Hooper NM (2011) Plasma alkaline phosphatase is elevated in Alzheimer's disease and inversely correlates with cognitive function. *Int J Mol Epidemiol Genet* 2:114–121
35. Thompson KH, McNeill JH, Orvig C (1999) Vanadium compounds as insulin mimics. *Chem Rev* 99:2561–2571. <https://doi.org/10.1021/cr980427c>
36. Dean RL (2002) Kinetic studies with alkaline phosphatase in the presence and absence of inhibitors and divalent cations. *Biochem. Mol Biol Educ* 30:401–407. <https://doi.org/10.1002/bmb.2002.494030060138>
37. Gellatly KS, Moorhead GBC, Duff SMC, Lefebvre DD, Plaxton WC (1994) Purification and characterization of a potato tuber. Acid phosphatase having significant phosphotyrosine phosphatase activity. *Plant Physiol* 106:223–232. <https://doi.org/10.1104/pp.106.1.223>
38. Schenk G, Miti N, Hanson GR, Comba P (2013) Purple acid phosphatase: a journey into the function and mechanism of a colorful enzyme. *Coord Chem Rev* 257:473–482. <https://doi.org/10.1016/j.ccr.2012.03.020>
39. Rane SY, Badave KD, Ahmed K (2009) Insight into bio-physiological functions of acid phosphatase from potatoes (*Solanum tuberosum*): a bioanalytical approach. *Indian J Chem* 48A:15–24
40. Kuftevec MM, Miller SA, Kuftevec MM, Miller SA (1972) Alkaline and acid phosphatase activities during growth of long bones and mandibles. *Calcif Tissue Res* 9:173–178. <https://doi.org/10.1007/BF02061955>
41. De la Iglesia IS, López-Jorge CE, Gómez-Casares MT, Lemes Castellano A, Cabrera PM, López Brito J, Suárez Cabrera A, Molero Labarta T (2009) Induction of apoptosis in leukemic cell lines treated with captopril, trandolapril and losartan: a new role in the treatment of leukaemia for these agents. *Leuk Res* 33:810–816. <https://doi.org/10.1016/j.leukres.2008.09.029>
42. Godugu C, Patel AR, Doddapaneni R, Marepally S, Jackson T, Singh M (2013) Inhalation delivery of Telmisartan enhances intratumoral distribution of nanoparticles in lung cancer models. *J Control Release* 172:86–95. <https://doi.org/10.1016/j.jconrel.2013.06.036>
43. Zhao W, Song Q, Zhang Z, Mao L, Zheng W, Hu X, Lian H (2015) The kinetic response of the proteome in A549 cells exposed to ZnSO₄ stress. *PLoS One* 10:e0133451. <https://doi.org/10.1371/journal.pone.0133451>

44. Jiang D, Sullivan PG, Sensi SL, Steward O, Weiss JH (2001) Zn(2+) induces permeability transition pore opening and release of pro-apoptotic peptides from neuronal mitochondria. *J Biol Chem* 276: 47524–47529
45. Donadelli M, Dalla Pozza E, Scupoli MT, Costanzo C, Scarpa A, Palmieri M (2009) Intracellular zinc increase inhibits p53^{-/-} pancreatic adenocarcinoma cell growth by ROS/AIF-mediated apoptosis. *Biochim Biophys Acta* 1793:273–280. <https://doi.org/10.1016/j.bbamcr.2008.09.010>
46. Yuan N, Wang YH, Li KJ, Zhao Y, Hu X, Mao L, Zhao WJ, Lian HZ, Zheng WJ (2012) Effects of exogenous zinc on the cellular zinc distribution and cell cycle of A549 cells. *Biosci Biotechnol Biochem* 76:2014–2020. <https://doi.org/10.1271/bbb.120216>
47. Goodsell DS (2002) The molecular perspective: Bcl-2 and apoptosis. *Stem Cells* 20:355–356. <https://doi.org/10.1634/stemcells.20-4-355>
48. Ku JH, Seo SY, Kwak C, Kim HH (2012) The role of survivin and Bcl-2 in zinc-induced apoptosis in prostate cancer cells. *Urol Oncol* 30:562–568. <https://doi.org/10.1016/j.urolonc.2010.06.001>
49. Etcheverry SB, Ferrer EG, Naso L, Barrio DA, Lezama L, Rojo T, Williams PAM (2007) Losartan and its interaction with copper(II): biological effects. *Bioorg Med Chem* 15:6418–6424